Measurement of the Photon Structure Function F_2^γ at Low x

The OPAL Collaboration

Abstract

Deep inelastic electron-photon scattering is studied using e^+e^- data collected by the OPAL detector at centre-of-mass energies $\sqrt{s_{ee}} \approx M_{Z^0}$. The photon structure function $F_2^\gamma(x, Q^2)$ is explored in a Q^2 range of 1.1 to 6.6 GeV^2 at lower x values than ever before. To probe this kinematic region events are selected with a beam electron scattered into one of the OPAL luminosity calorimeters at scattering angles between 27 and 55 mrad. A measurement is presented of the photon structure function $F_2^\gamma(x, Q^2)$ at $\langle Q^2 \rangle = 1.86$ GeV^2 and 3.76 GeV^2 in five logarithmic x bins from 0.0025 to 0.2.

(Submitted to Physics Letters B)

The OPAL Collaboration

K. Ackerstaff[8], G. Alexander[23], J. Allison[16], N. Altekamp[5], K.J. Anderson[9],
S. Anderson[12], S. Arcelli[2], S. Asai[24], D. Axen[29], G. Azuelos[18,a], A.H. Ball[17],
E. Barberio[8], T. Barillari[2], R.J. Barlow[16], R. Bartoldus[3], J.R. Batley[5], S. Baumann[3],
J. Bechtluft[14], C. Beeston[16], T. Behnke[8], A.N. Bell[1], K.W. Bell[20], G. Bella[23],
S. Bentvelsen[8], S. Bethke[14], O. Biebel[14], A. Biguzzi[5], S.D. Bird[16], V. Blobel[27],
I.J. Bloodworth[1], J.E. Bloomer[1], M. Bobinski[10], P. Bock[11], D. Bonacorsi[2],
M. Boutemeur[34], B.T. Bouwens[12], S. Braibant[12], L. Brigliadori[2], R.M. Brown[20],
H.J. Burckhart[8], C. Burgard[8], R. Bürgin[10], P. Capiluppi[2], R.K. Carnegie[6],
A.A. Carter[13], J.R. Carter[5], C.Y. Chang[17], D.G. Charlton[1,b], D. Chrisman[4],
P.E.L. Clarke[15], I. Cohen[23], J.E. Conboy[15], O.C. Cooke[8], M. Cuffiani[2], S. Dado[22],
C. Dallapiccola[17], G.M. Dallavalle[2], R. Davies[30], S. De Jong[12], L.A. del Pozo[4],
K. Desch[3], B. Dienes[33,d], M.S. Dixit[7], E. do Couto e Silva[12], M. Doucet[18],
E. Duchovni[26], G. Duckeck[34], I.P. Duerdoth[16], D. Eatough[16], J.E.G. Edwards[16],
P.G. Estabrooks[6], H.G. Evans[9], M. Evans[13], F. Fabbri[2], M. Fanti[2], A.A. Faust[30],
F. Fiedler[27], M. Fierro[2], H.M. Fischer[3], I. Fleck[8], R. Folman[26], D.G. Fong[17],
M. Foucher[17], A. Fürtjes[8], D.I. Futyan[16], P. Gagnon[7], J.W. Gary[4], J. Gascon[18],
S.M. Gascon-Shotkin[17], N.I. Geddes[20], C. Geich-Gimbel[3], T. Geralis[20], G. Giacomelli[2],
P. Giacomelli[4], R. Giacomelli[2], V. Gibson[5], W.R. Gibson[13], D.M. Gingrich[30,a],
D. Glenzinski[9], J. Goldberg[22], M.J. Goodrick[5], W. Gorn[4], C. Grandi[2], E. Gross[26],
J. Grunhaus[23], M. Gruwé[8], C. Hajdu[32], G.G. Hanson[12], M. Hansroul[8], M. Hapke[13],
C.K. Hargrove[7], P.A. Hart[9], C. Hartmann[3], M. Hauschild[8], C.M. Hawkes[5],
R. Hawkings[27], R.J. Hemingway[6], M. Herndon[17], G. Herten[10], R.D. Heuer[8],
M.D. Hildreth[8], J.C. Hill[5], S.J. Hillier[1], P.R. Hobson[25], R.J. Homer[1], A.K. Honma[28,a],
D. Horváth[32,c], K.R. Hossain[30], R. Howard[29], P. Hüntemeyer[27], D.E. Hutchcroft[5],
P. Igo-Kemenes[11], D.C. Imrie[25], M.R. Ingram[16], K. Ishii[24], A. Jawahery[17],
P.W. Jeffreys[20], H. Jeremie[18], M. Jimack[1], A. Joly[18], C.R. Jones[5], G. Jones[16],
M. Jones[6], U. Jost[11], P. Jovanovic[1], T.R. Junk[8], D. Karlen[6], V. Kartvelishvili[16],
K. Kawagoe[24], T. Kawamoto[24], P.I. Kayal[30], R.K. Keeler[28], R.G. Kellogg[17],
B.W. Kennedy[20], J. Kirk[29], A. Klier[26], S. Kluth[8], T. Kobayashi[24], M. Kobel[10],
D.S. Koetke[6], T.P. Kokott[3], M. Kolrep[10], S. Komamiya[24], T. Kress[11], P. Krieger[6],
J. von Krogh[11], P. Kyberd[13], G.D. Lafferty[16], R. Lahmann[17], W.P. Lai[19], D. Lanske[14],
J. Lauber[15], S.R. Lautenschlager[31], J.G. Layter[4], D. Lazic[22], A.M. Lee[31], E. Lefebvre[18],
D. Lellouch[26], J. Letts[12], L. Levinson[26], S.L. Lloyd[13], F.K. Loebinger[16], G.D. Long[28],
M.J. Losty[7], J. Ludwig[10], A. Macchiolo[2], A. Macpherson[30], M. Mannelli[8],
S. Marcellini[2], C. Markus[3], A.J. Martin[13], J.P. Martin[18], G. Martinez[17], T. Mashimo[24],
P. Mättig[3], W.J. McDonald[30], J. McKenna[29], E.A. Mckigney[15], T.J. McMahon[1],
R.A. McPherson[8], F. Meijers[8], S. Menke[3], F.S. Merritt[9], H. Mes[7], J. Meyer[27],
A. Michelini[2], G. Mikenberg[26], D.J. Miller[15], A. Mincer[22,e], R. Mir[26], W. Mohr[10],
A. Montanari[2], T. Mori[24], M. Morii[24], U. Müller[3], S. Mihara[24], K. Nagai[26],
I. Nakamura[24], H.A. Neal[8], B. Nellen[3], R. Nisius[8], S.W. O'Neale[1], F.G. Oakham[7],
F. Odorici[2], H.O. Ogren[12], A. Oh[27], N.J. Oldershaw[16], M.J. Oreglia[9], S. Orito[24],
J. Pálinkás[33,d], G. Pásztor[32], J.R. Pater[16], G.N. Patrick[20], J. Patt[10], M.J. Pearce[1],

1

R. Perez-Ochoa[8], S. Petzold[27], P. Pfeifenschneider[14], J.E. Pilcher[9], J. Pinfold[30], D.E. Plane[8], P. Poffenberger[28], B. Poli[2], A. Posthaus[3], D.L. Rees[1], D. Rigby[1], S. Robertson[28], S.A. Robins[22], N. Rodning[30], J.M. Roney[28], A. Rooke[15], E. Ros[8], A.M. Rossi[2], P. Routenburg[30], Y. Rozen[22], K. Runge[10], O. Runolfsson[8], U. Ruppel[14], D.R. Rust[12], R. Rylko[25], K. Sachs[10], T. Saeki[24], E.K.G. Sarkisyan[23], C. Sbarra[29], A.D. Schaile[34], O. Schaile[34], F. Scharf[3], P. Scharff-Hansen[8], P. Schenk[34], J. Schieck[11], P. Schleper[11], B. Schmitt[8], S. Schmitt[11], A. Schöning[8], M. Schröder[8], H.C. Schultz-Coulon[10], M. Schumacher[3], C. Schwick[8], W.G. Scott[20], T.G. Shears[16], B.C. Shen[4], C.H. Shepherd-Themistocleous[8], P. Sherwood[15], G.P. Siroli[2], A. Sittler[27], A. Skillman[15], A. Skuja[17], A.M. Smith[8], G.A. Snow[17], R. Sobie[28], S. Söldner-Rembold[10], R.W. Springer[30], M. Sproston[20], K. Stephens[16], J. Steuerer[27], B. Stockhausen[3], K. Stoll[10], D. Strom[19], P. Szymanski[20], R. Tafirout[18], S.D. Talbot[1], S. Tanaka[24], P. Taras[18], S. Tarem[22], R. Teuscher[8], M. Thiergen[10], M.A. Thomson[8], E. von Törne[3], S. Towers[6], I. Trigger[18], Z. Trócsányi[33], E. Tsur[23], A.S. Turcot[9], M.F. Turner-Watson[8], P. Utzat[11], R. Van Kooten[12], M. Verzocchi[10], P. Vikas[18], E.H. Vokurka[16], H. Voss[3], F. Wäckerle[10], A. Wagner[27], C.P. Ward[5], D.R. Ward[5], P.M. Watkins[1], A.T. Watson[1], N.K. Watson[1], P.S. Wells[8], N. Wermes[3], J.S. White[28], B. Wilkens[10], G.W. Wilson[27], J.A. Wilson[1], G. Wolf[26], T.R. Wyatt[16], S. Yamashita[24], G. Yekutieli[26], V. Zacek[18], D. Zer-Zion[8]

[1]School of Physics and Space Research, University of Birmingham, Birmingham B15 2TT, UK
[2]Dipartimento di Fisica dell' Università di Bologna and INFN, I-40126 Bologna, Italy
[3]Physikalisches Institut, Universität Bonn, D-53115 Bonn, Germany
[4]Department of Physics, University of California, Riverside CA 92521, USA
[5]Cavendish Laboratory, Cambridge CB3 0HE, UK
[6] Ottawa-Carleton Institute for Physics, Department of Physics, Carleton University, Ottawa, Ontario K1S 5B6, Canada
[7]Centre for Research in Particle Physics, Carleton University, Ottawa, Ontario K1S 5B6, Canada
[8]CERN, European Organisation for Particle Physics, CH-1211 Geneva 23, Switzerland
[9]Enrico Fermi Institute and Department of Physics, University of Chicago, Chicago IL 60637, USA
[10]Fakultät für Physik, Albert Ludwigs Universität, D-79104 Freiburg, Germany
[11]Physikalisches Institut, Universität Heidelberg, D-69120 Heidelberg, Germany
[12]Indiana University, Department of Physics, Swain Hall West 117, Bloomington IN 47405, USA
[13]Queen Mary and Westfield College, University of London, London E1 4NS, UK
[14]Technische Hochschule Aachen, III Physikalisches Institut, Sommerfeldstrasse 26-28, D-52056 Aachen, Germany
[15]University College London, London WC1E 6BT, UK
[16]Department of Physics, Schuster Laboratory, The University, Manchester M13 9PL, UK
[17]Department of Physics, University of Maryland, College Park, MD 20742, USA

[18]Laboratoire de Physique Nucléaire, Université de Montréal, Montréal, Quebec H3C 3J7, Canada
[19]University of Oregon, Department of Physics, Eugene OR 97403, USA
[20]Rutherford Appleton Laboratory, Chilton, Didcot, Oxfordshire OX11 0QX, UK
[22]Department of Physics, Technion-Israel Institute of Technology, Haifa 32000, Israel
[23]Department of Physics and Astronomy, Tel Aviv University, Tel Aviv 69978, Israel
[24]International Centre for Elementary Particle Physics and Department of Physics, University of Tokyo, Tokyo 113, and Kobe University, Kobe 657, Japan
[25]Brunel University, Uxbridge, Middlesex UB8 3PH, UK
[26]Particle Physics Department, Weizmann Institute of Science, Rehovot 76100, Israel
[27]Universität Hamburg/DESY, II Institut für Experimental Physik, Notkestrasse 85, D-22607 Hamburg, Germany
[28]University of Victoria, Department of Physics, P O Box 3055, Victoria BC V8W 3P6, Canada
[29]University of British Columbia, Department of Physics, Vancouver BC V6T 1Z1, Canada
[30]University of Alberta, Department of Physics, Edmonton AB T6G 2J1, Canada
[31]Duke University, Dept of Physics, Durham, NC 27708-0305, USA
[32]Research Institute for Particle and Nuclear Physics, H-1525 Budapest, P O Box 49, Hungary
[33]Institute of Nuclear Research, H-4001 Debrecen, P O Box 51, Hungary
[34]Ludwigs-Maximilians-Universität München, Sektion Physik, Am Coulombwall 1, D-85748 Garching, Germany

[a] and at TRIUMF, Vancouver, Canada V6T 2A3
[b] and Royal Society University Research Fellow
[c] and Institute of Nuclear Research, Debrecen, Hungary
[d] and Department of Experimental Physics, Lajos Kossuth University, Debrecen, Hungary
[e] and Department of Physics, New York University, NY 1003, USA

The hadronic structure function F_2^γ of the photon has been measured in deep inelastic electron-photon scattering at various e^+e^- experiments ([2,4,3,1] and references therein). In the previous OPAL analysis [1] $F_2^\gamma(x, Q^2)$ was measured using tagged electrons with a range of scattering angles from 60 mrad up to 500 mrad to the initial beam direction. This letter describes an analysis of data collected in 1993 and 1994 at e^+e^- center-of-mass energies between 89.2 GeV and 93.2 GeV, using the OPAL silicon tungsten (SW) luminometer as the electron tagger with a clear angular acceptance from 27 mrad to 55 mrad. This corresponds to a lowest Q^2 value of 1.14 GeV^2 in the selected sample, close to the lower limit at which perturbative QCD can be expected to work. The energy of the LEP beams is higher than at any previous e^+e^- collider so lower values of the scaling variable x can be reached at any given Q^2. The results reported

3

here go down to $x = 0.0025$. This kinematical region is of particular interest because theoretical predictions differ significantly from each other [5–11] and because in this region the proton structure function is observed to start to increase as x decreases [12].

In the singly-tagged regime, with one scattered electron tagged in the detector, the two photon process can be regarded as the deep inelastic scattering of an $e^{\pm}$ with four-momentum k on a quasi-real photon with four-momentum p. The flux of quasi-real photons can be calculated using the Equivalent Photon Approximation [13]. The cross-section for deep inelastic electron-photon scattering with a hadronic final state X is expressed as [14],

$$\frac{d^2\sigma_{e\gamma \to eX}}{dx\,dQ^2} = \frac{2\pi\alpha^2}{x\,Q^4} \left[\left(1 + (1-y)^2\right) F_2^\gamma(x, Q^2) - y^2 F_L^\gamma(x, Q^2) \right] , \tag{1}$$

where $Q^2 \equiv -q^2$ is the negative four-momentum squared of the virtual photon and α is the fine structure constant. The usual dimensionless variables of deep inelastic scattering, x and y, are defined as

$$x \equiv \frac{Q^2}{2\,p \cdot q} , \quad y \equiv \frac{p \cdot q}{p \cdot k}. \tag{2}$$

In the kinematic regime studied here ($y^2 \ll 1$) the contribution of the term proportional to the longitudinal structure function $F_L^\gamma(x, Q^2)$ is small and is therefore neglected. The structure function formalism of deep inelastic scattering implies that the virtual photon behaves as a pointlike probe. However, at very low Q^2 it can also show a hadronic structure. For this analysis, such a hadronic contribution is neglected.

The scattered electron is detected with the silicon tungsten calorimeters (SW) [15] that are placed around the beam pipe at a distance of 2.4 m in z from the interaction point on both sides of the OPAL detector, covering polar angles θ from 25 to 59 mrad[1]. They are cylindrical sampling calorimeters consisting of 19 layers of silicon detectors interleaved with 18 layers of tungsten, equivalent to a total of 22 radiation lengths. For electromagnetic showers an energy resolution of $24\%/\sqrt{E\,[\text{GeV}]}$ and a resolution in polar angle of 0.06 mrad is achieved. The hadronic final state X is measured with SW, the forward detectors FD, the OPAL electromagnetic calorimeter and the OPAL tracking system which consists of a silicon microvertex detector, a drift chamber vertex detector, a jet chamber and z-chambers [16].

The measurement of $F_2^\gamma(x, Q^2)$ involves the determination of Q^2 and x that can be obtained from the four-vectors of the tagged electron and the hadronic final state:

$$Q^2 \approx 2\,E_b\,E_{\text{tag}}\,(1 - \cos\theta_{\text{tag}}) \qquad \text{(neglecting the electron mass)} \tag{3}$$

$$x \approx \frac{Q^2}{Q^2 + W^2} \qquad \text{(for } P^2 \equiv -p^2 \approx 0\text{)}. \tag{4}$$

---

[1]A right-handed coordinate system is used. The x-axis points towards the centre of the LEP ring, the y-axis upwards and the z-axis in the direction of the electron beam. The polar angle θ and the azimuthal angle ϕ are defined with respect to the z-axis and x-axis, respectively.

E_{tag} and θ_{tag} are the energy and polar angle of the observed electron, E_{b} is the beam energy, and W the invariant mass of the hadronic final state. In addition to the tag requirement, an antitag condition is applied to ensure that the virtuality of the quasi-real photon P^2 is small and requirements are imposed on the hadronic final state to reject residual background.

1. A tagged electron is required, identified as a cluster in the silicon tungsten calorimeter with energy $0.775\,E_{\mathrm{b}} \leq E_{\mathrm{tag}} \leq 1.2\,E_{\mathrm{b}}$ and a polar angle $27 \leq \theta_{\mathrm{tag}} \leq 55$ mrad with respect to the beam axis, defining a lower limit of $Q^2_{\mathrm{min}} = 1.14$ GeV^2 and an upper limit of $Q^2_{\mathrm{max}} = 6.57$ GeV^2
   (tag requirement).

2. The energy E_{at} of the most energetic cluster in the hemisphere opposite to the one containing the tagged electron is restricted to $E_{\mathrm{at}} \leq 0.25\,E_{\mathrm{b}}$
   (antitag requirement).

3. The visible invariant mass W_{vis} of the hadronic system is required to be in the range $2.5\,\mathrm{GeV} \leq W_{\mathrm{vis}} \leq 40\,\mathrm{GeV}$. W_{vis} is defined by all tracks of charged particles and all calorimeter clusters which are not associated with tracks, including clusters from FD and SW but excluding the tagged electron. The same quality criteria are applied to all calorimeter clusters and charged tracks as in the previous analysis [1]. The masses of all particles in the hadronic system are assumed to be equal to the pion mass.

4. $N_{\mathrm{ch}} > 2$, where N_{ch} is the number of charged particle tracks originating from the hadronic final state.

5. The transverse momentum component $p_{\mathrm{t}}^{\mathrm{bal}}$ of the event parallel to the tag plane has to be lower than 3 GeV. The tag plane is defined by the momentum vectors of the incoming beam electron and the tagged electron. The transverse momentum of the event is the vector sum of the momenta perpendicular to the beam axis of all measured particles, including the tagged electron.

6. The transverse momentum component of the hadronic system perpendicular to the tag plane $p_{\mathrm{t}}^{\mathrm{out}}$ has to be lower than 3 GeV.

These requirements select 7112 events, corresponding to an integrated luminosity of 70.8 ± 0.2 pb^{-1}, with $\langle Q^2 \rangle = 2.8$ GeV^2. Using sets of independent triggers, the trigger efficiency was evaluated to be $(98 \pm 2)\%$.

The dominant background comes from two-photon events with a lepton pair in the final state. These events are simulated with the Vermaseren Monte Carlo generator [17]. Background from other sources such as other QED processes with four fermions in the final state or the process $Z^0 \rightarrow$ hadrons is found to be below 0.5%. The total estimated background contamination in the selected sample is $(2.5 \pm 0.2)\%$. Deep inelastic electron-photon scattering is simulated with the generators HERWIG 5.18d

5

[18], PYTHIA 5.722 [19] and F2GEN [20]. F2GEN includes two final state models, "pointlike" and "peripheral", to describe the hard and soft limit of the process (see Ref. [1] for details). All Monte Carlo events are passed through a detailed detector simulations program [21] and the same reconstruction and analysis chain as the real data events.

In Ref. [1] several distributions of measured final state hadronic quantities were studied in the Q^2 range $4.6\,\mathrm{GeV}^2 < Q^2 < 30\,\mathrm{GeV}^2$, and significant differences were observed, both between data and the Monte Carlo models, and between the different Monte Carlo models. These distributions have been re-examined in the different kinematic range of this analysis and a similar pattern of disagreements is seen, especially in the energy flow distributions (Figure 1), and in the summed transverse energy perpendicular to the tag plane. These differences are found to be most prominent for $x_{\mathrm{vis}} < 0.05$, and small at higher x_{vis}. (The peripheral final state model of F2GEN has a similar behaviour to PYTHIA and is not shown.) Such uncertainties in the modelling of the hadronic final state give rise to uncertainties in the unfolded $F_2^\gamma(x, Q^2)$ [1]. They are included in the systematic error using the same set of Monte Carlo models as in Ref. [1], except for the F2GEN models. For F2GEN, a weighted mixture of the two final state models available in the generator is used throughout the analysis. This mixture has been optimised to improve the final state description by a fit to the hadronic energy flow of the data in the lowest x bin. To account for the uncertainty of this 'ad hoc' procedure a variation of the fit by $\pm$ three times its error is included in the evaluation of the systematic error.

The program RUN by Blobel [22] is used to unfold the structure function F_2^γ from the measured x_{vis} distribution. To resolve very low x values the unfolding is performed on a logarithmic x scale.

The ability of the unfolding to recover the underlying structure function F_2^γ of the data is tested by unfolding the known structure function of Monte Carlo samples, the "mock data", instead of measured data. These mock data samples are then unfolded with other Monte Carlo sample. The unfolded F_2^γ functions are compared to the original structure functions used in the generation of the mock data sample. Figure 2(a) and (b) show unfoldings of a mock data sample generated with the HERWIG generator and the GRV-LO [5] parton density functions using unfolding Monte Carlo samples from different generators and different input structure functions. The samples are divided into two Q^2 bins with (a) $Q^2 < 2.5\,\mathrm{GeV}^2$ and (b) $Q^2 > 2.5\,\mathrm{GeV}^2$, respectively. The error bars include statistical errors only. The solid line is the GRV-LO structure function for the average Q^2 of the mock data sample. Figure 2(c) and (d) show similar plots for a mock data sample generated with HERWIG and the DG [6] structure function. Here, the solid line is the DG structure function.

The deviations observed represent the systematic impact on the unfolded result of different parton density functions and modelling of the hadronic final state. The DG structure function is used as a test for an F_2^γ function that vanishes for $x \to 0$. The DG parton density functions have been evolved by their authors from $Q_0^2 = 4.0\,\mathrm{GeV}^2$ [6]

6

and are not supposed to be valid at lower Q^2, but they are suitable for this purely technical purpose. Figure 2(a) and (c) demonstrate that despite the systematic errors originating from different Monte Carlo models a structure function falling for $x \to 0$ could be measured and distinguished from the GRV-LO prediction in the lower Q^2 bin. In the higher Q^2 bin the systematic errors are larger: The spread of the unfolding results shown in Figure 2(d) does not allow the exclusion of the F_2^γ function described by GRV-LO.

To determine the central values of the measured F_2^γ a "reference" unfolding is defined. It is based on a HERWIG sample generated using the GRV-LO parametrisation, chosen for consistency with previous OPAL results [1]. The event selection as described above is applied. The data are divided into two Q^2 bins with $Q^2 < 2.5$ GeV^2 and $Q^2 > 2.5$ GeV^2 which are unfolded separately. The two bins contain approximately equal numbers of events. The x binning is chosen to keep correlations low between the unfolded F_2^γ values in the different x bins.

The Monte Carlo generators HERWIG and F2GEN predict mean values of $\langle P^2 \rangle = 0.03 - 0.08$ GeV^2 for the virtuality of the quasi-real photon, depending on the model and the structure function used. Several theoretical predictions exist for how F_2^γ should behave as a function of P^2 [24, 23, 25]. An estimate for the effect of the non-zero virtuality P^2 yields an increase of F_2^γ by roughly 10%, based on the P^2 dependent structure function parameterisation of Schuler and Sjöstrand [23] and the reference Monte Carlo sample. As the distribution of P^2 in the data and the correct theoretical prescription are not known, no correction is applied to the results.

Q^2 [GeV^2]	$\langle Q^2 \rangle$ [GeV^2]	x range		x (centre of $\log_{10}(x)$ bin)	F_2^γ / α
		$-\log_{10}(x)$	x		
$1.1 - 2.5$	1.86	$2.6 - 2.2$	$0.0025 - 0.0063$	0.004	$0.27 \pm 0.03 \, {}^{+0.05}_{-0.07}$
		$2.2 - 1.7$	$0.0063 - 0.020$	0.011	$0.22 \pm 0.02 \, {}^{+0.02}_{-0.05}$
		$1.7 - 1.4$	$0.020 \ \ - 0.040$	0.028	$0.20 \pm 0.02 \, {}^{+0.09}_{-0.02}$
		$1.4 - 1.0$	$0.040 \ \ - 0.100$	0.063	$0.23 \pm 0.02 \, {}^{+0.03}_{-0.05}$
$2.5 - 6.6$	3.76	$2.2 - 1.7$	$0.0063 - 0.020$	0.011	$0.35 \pm 0.03 \, {}^{+0.08}_{-0.08}$
		$1.7 - 1.4$	$0.020 \ \ - 0.040$	0.028	$0.29 \pm 0.03 \, {}^{+0.06}_{-0.06}$
		$1.4 - 1.0$	$0.040 \ \ - 0.100$	0.063	$0.32 \pm 0.02 \, {}^{+0.07}_{-0.05}$
		$1.0 - 0.7$	$0.100 \ \ - 0.200$	0.141	$0.32 \pm 0.03 \, {}^{+0.08}_{-0.04}$

Table 1: Results for F_2^γ as a function of x in bins of Q^2. The first errors is statistical and the second systematic. The systematic errors do not contain the systematic effect caused by P^2 being different from zero.

The unfolded F_2^γ / α for the data is listed in Table 1, and shown in Figure 3. The value of F_2^γ / α is given at the centre of each bin in $\log_{10}(x)$. The error bars show

both the statistical error alone and the quadratic sum of statistical and systematic errors. Figure 3 also shows the F_2^γ/α calculated from the GRV-LO and the SaS-1D [7] leading order parton density parametrisations and the higher order GRV-HO [5] parametrisation, evaluated at the corresponding $\langle Q^2 \rangle$ values. The parton density parametrisations given in Ref. [8–11] are not shown because they are not supposed to be valid at these Q^2 values, similarly to the DG parametrisation. In addition results from PLUTO [2] and TPC/2γ [4] for similar Q^2 values are shown for comparison.

The central values and statistical errors of the F_2^γ measurements are determined using the reference unfolding. The statistical errors include, in addition to the statistical error of the measured data, also the error due to the limited number of Monte Carlo events (1.6 times the number of data events) which is estimated to be $1/\sqrt{1.6}$ times the statistical error of the measured data. The estimation of the systematic errors includes the following four components:

- The selection requirements are varied in order to change the signal and background event composition and to take into account possible uncertainties in the simulation of variables which are used for the event selection. The size of the variations reflects the resolution of the measured variable and fulfils the requirement that the mean $\langle Q^2 \rangle$ of the sample is not shifted significantly by the variation.

- An altered set of quality criteria for calorimeter clusters and tracks is used to determine systematic errors resulting from imperfections in the simulation of the detector acceptance and calibration for tracks and calorimeter clusters.

- The unfolding is performed using the HERWIG generator and the standard selection, but replacing the GRV-LO parton density functions with SaS-1D in order to study the uncertainty due to the structure functions assumed in the Monte Carlo samples.

- The unfolding is performed with the standard selection requirements using PYTHIA and F2GEN in order to study the effect due to a different modelling of the hadronic final state in the different Monte Carlo programs.

For each of the four systematic studies, the maximum deviations (above and below) of the various unfolding results from the result of the reference unfolding are taken as systematic errors. The total systematic error assigned to the results in Table 1 is the quadratic sum of these four contributions.

In summary, OPAL data recorded in 1993 and 1994 have been used to measure the photon structure function $F_2^\gamma(x, Q^2)$ at low x using events with an electron tagged in the silicon tungsten calorimeters. $F_2^\gamma(x, Q^2)$ has been unfolded as a function of x in two bins of Q^2, with $\langle Q^2 \rangle = 1.86$ and $3.76\,\mathrm{GeV}^2$. The unfolding has been performed on a logarithmic x scale to resolve the lowest accessible x values. The data have been unfolded down to a minimum x of 0.0025, lower than measured previously [2, 4, 3, 1]. This is the region where the proton structure function as measured at HERA starts to

rise [12]. The extracted F_2^γ result is consistent with the other OPAL F_2^γ measurements [1, 26]. Within errors the results agree with the lowest value published by PLUTO [2]. Compared to the TPC/2γ measurement [4] our results tend to be higher. Our result is consistent with a flat $F_2^\gamma(x)$ in both Q^2 ranges within the errors though it does not exclude a small rise with decreasing x. The unfolded result is consistent in shape with the GRV-LO and SaS-1D parameterisations for the corresponding Q^2 values. However, the measured F_2^γ is higher than the GRV-LO and SaS-1D predictions. The GRV-HO prediction follows the data more closely and is in good agreement in the lower Q^2 bin.

Acknowledgements

References

[1] OPAL Collaboration, K. Ackerstaff *et al.*, Z. Phys. **C74** (1997) 33.

[2] PLUTO Collaboration, C. Berger *et al.*, Phys. Lett. **B142** (1984) 111.

[3] TASSO Collaboration, M. Althoff *et al.*, Z. Phys. **C31** (1986) 527.

[4] TPC/2γ Collaboration, H. Aihara *et al.*, Z. Phys. **C34** (1987) 1.

[5] M. Glück, E. Reya and A. Vogt, Phys. Rev. **D46** (1992) 1973;
M. Glück, E. Reya and A. Vogt, Phys. Rev. **D45** (1992) 3986.

[6] M. Drees, K. Grassie, Z. Phys. **C28** (1985) 451.

[7] G. A. Schuler and T. Sjöstrand, Z. Phys. **C68** (1995) 607.

[8] L.E. Gordon, J.K. Storrow, Z. Phys. **C56** (1992) 307.

[9] K. Hagiwara, M. Tanaka, I. Watanabe, Phys. Rev. **D51** (1995) 3197.

[10] H. Abramowicz, K. Charchula, A. Levy, Phys. Lett. **B269** (1991) 458.

[11] F. Kapusta, Z. Phys. **C42** (1989) 225.

[12] H1 Collaboration, C. Adloff *et al.*, DESY 97-042, 1997;
ZEUS Collaboration, M. Derrick *et al.*, Z. Phys. **C69** (1996) 607.

[13] C. F. von Weizsäcker, Z. Phys. **88** (1934) 612;
E. J. Williams, Phys. Rev. **45** (1934) 729;
V. M. Budnev *et al.*, Phys. Rep. **15** (1975) 181.

[14] C. Berger and W. Wagner, Phys. Rep. **146** (1987) 1.

[15] B. E. Anderson *et al.*, IEEE Transactions on Nuclear Science **41** (1994) 845.

[16] OPAL Collaboration, K. Ahmet *et al.*, Nucl. Instr. and Meth. **A305** (1991) 275;
P. P. Allport *et al.*, Nucl. Instr. and Meth. **A346** (1994) 476.

[17] J. A. M. Vermaseren, Nucl. Phys. **B229** (1983) 347;
J. A. M. Vermaseren, J. Smith and G. Grammer Jr., Phys. Rev. **D19** (1979) 137.

[18] G. Marchesini *et al.*, Comp. Phys. Comm. **67** (1992) 465.

[19] T. Sjöstrand, Comp. Phys. Comm. **82** (1994) 74.

[20] A. Buijs *et al.*, Comp. Phys. Comp. **79** (1994) 523;
J. J. Ward, PhD Thesis, University College London UCL (1996), unpublished.

[21] J. Allison *et al.*, Nucl. Instr. and Meth. **A317** (1992) 47.

[22] V. Blobel, DESY-84-118, 1984.

[23] G. A. Schuler and T. Sjöstrand, Phys. Lett. **B376** (1996) 193.

[24] M. Glück, E. Reya and M. Stratmann, Phys. Rev. **D51** (1995) 3220;
M. Glück, E. Reya and M. Stratmann, Phys. Rev. **D54** (1996) 5515.

[25] M. Drees and R. M. Godbole, Phys. Rev. **D50** (1994) 3124.

[26] OPAL Collaboration, K. Ackerstaff *et al.*, CERN-PPE/97-087, submitted to Phys. Lett. **B**.
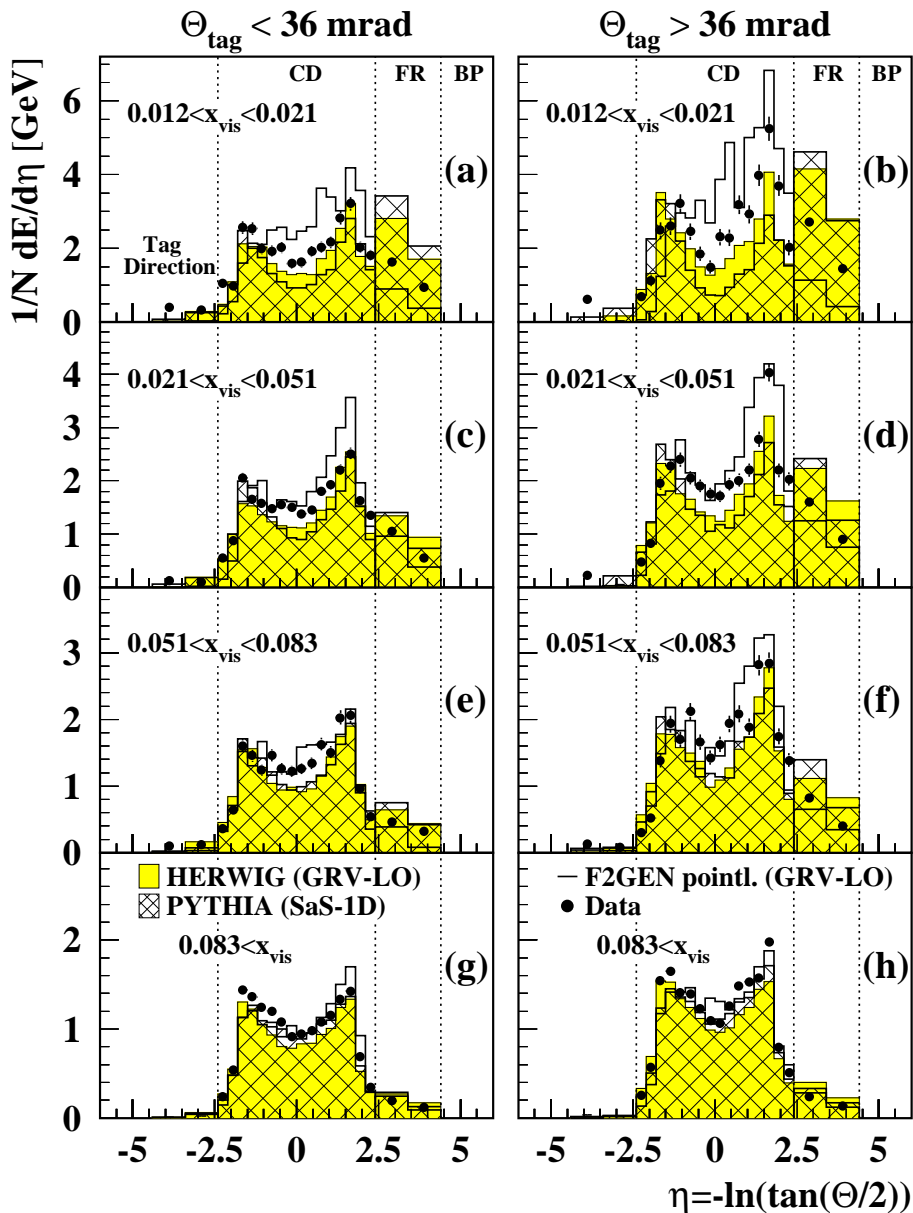
OPAL

Figure 1: The hadronic energy flow per event as a function of pseudorapidity η for the data and various Monte Carlo samples. In (a)-(f) the values of the bin limits in x_{vis} have been derived from the bin limits in x_{true} of the three lowest x bins in Figure 3(a). The bins in θ_{tag} correspond approximately to the Q^2 bins of the unfolding. The errors shown are statistical only. The vertical lines show the acceptance regions of the OPAL detector components, CD = Central Detector, FR = Forward Region and BP = Beam Pipe. (FR, BP not marked on the tag side).
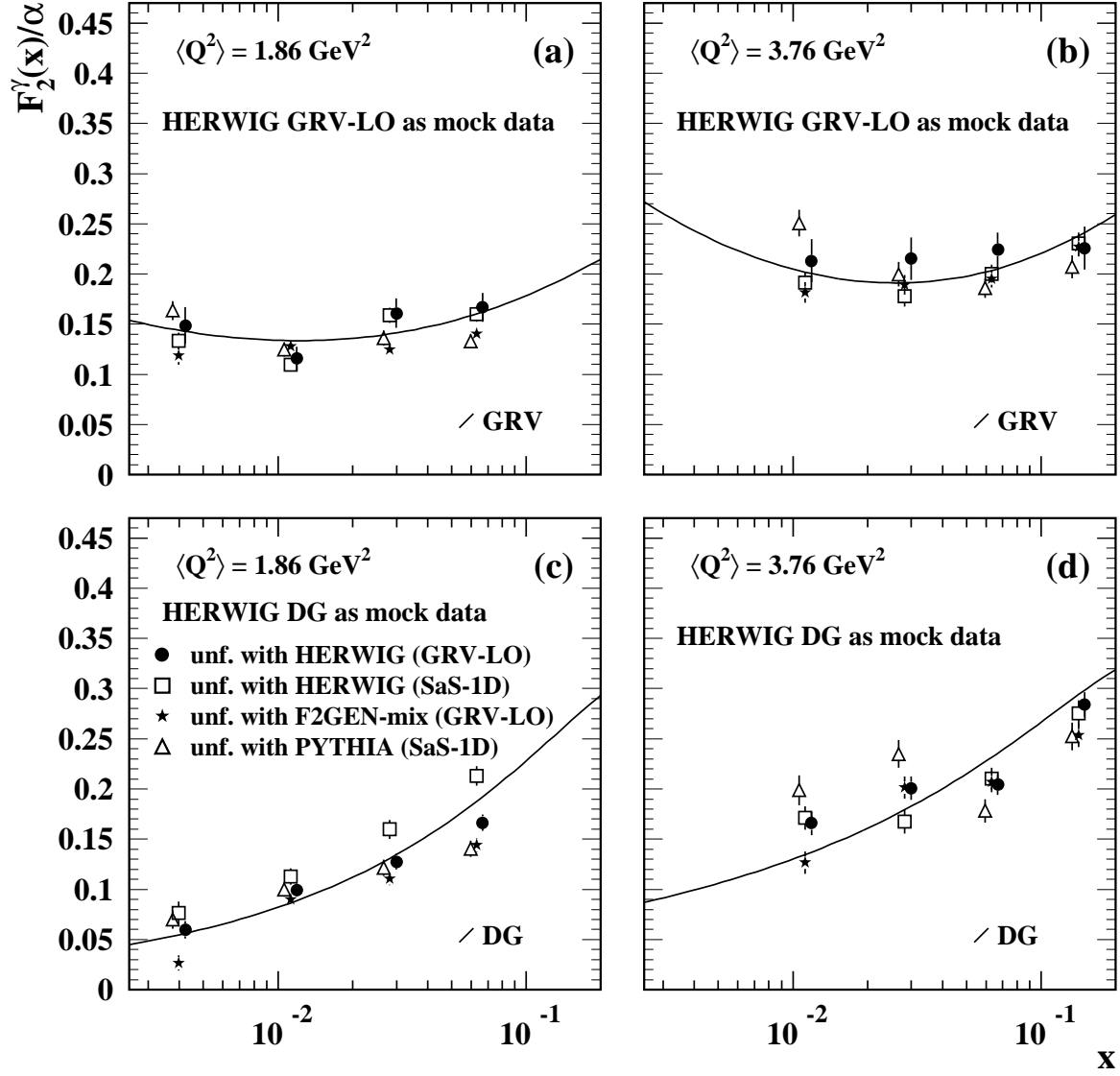
Figure 2: Unfolding tests: In (a) and (b) mock data samples of HERWIG events with the GRV-LO parton density functions were unfolded using one of the four listed unfolding Monte Carlo samples. The solid curves show the GRV-LO $F_2^\gamma(x)$ for $Q^2 = 1.86\,\mathrm{GeV}^2$ and $Q^2 = 3.76\,\mathrm{GeV}^2$. In (c) and (d) a similar exercise was performed with mock data samples from HERWIG with the DG parton density functions. The solid curves show the corresponding DG values for $F_2^\gamma(x)$ at $Q^2 = 1.86\,\mathrm{GeV}^2$ and $Q^2 = 3.76\,\mathrm{GeV}^2$. The error bars are statistical only. The symbols are slightly shifted in x to avoid overlap.
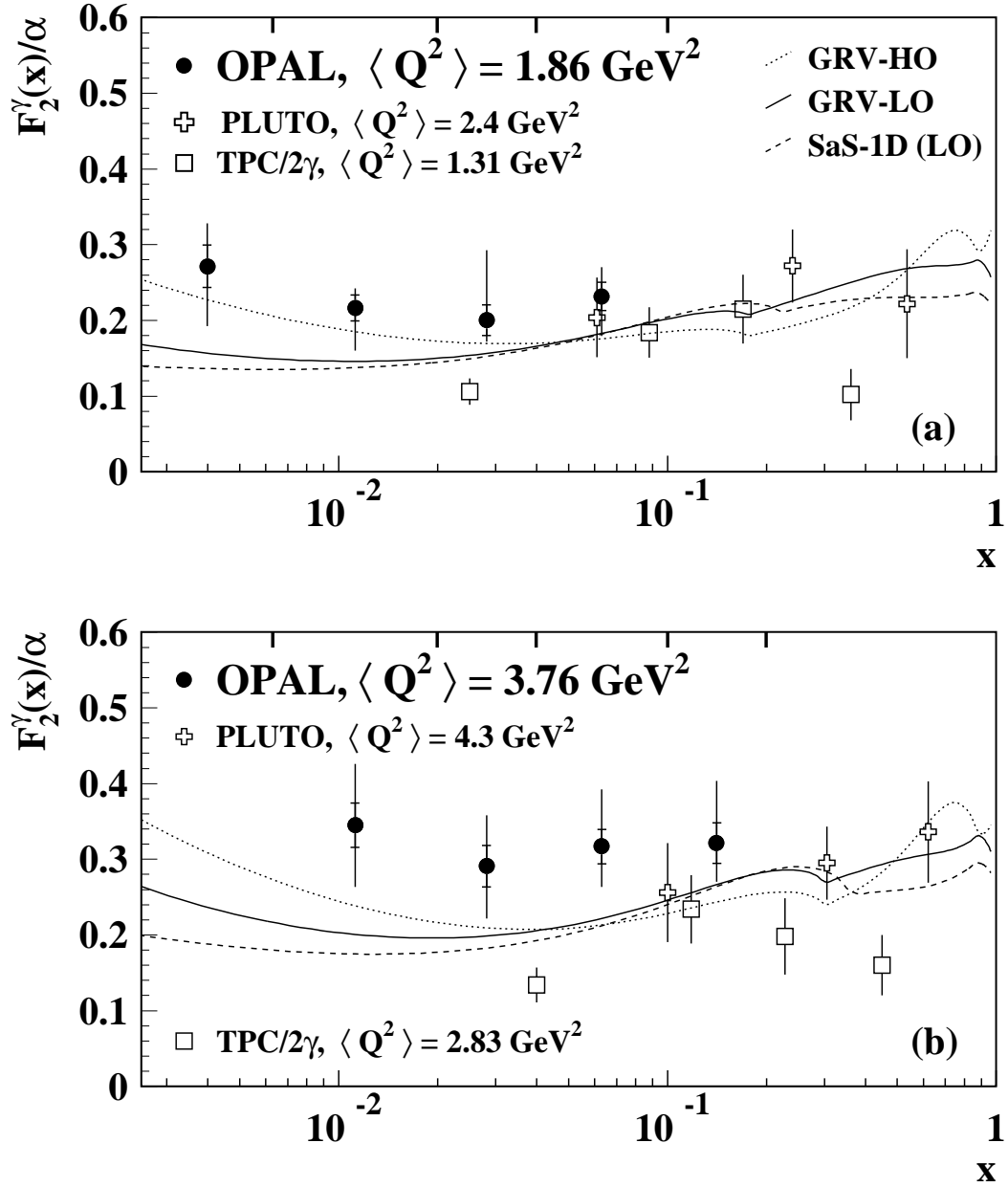
Figure 3: The full circles show our result for $F_2^\gamma(x)$ at $\langle Q^2 \rangle = 1.86\,\mathrm{GeV}^2$ (a) and $\langle Q^2 \rangle = 3.76\,\mathrm{GeV}^2$ (b). The total error and the statistical contribution are shown for each point. The tick marks at the top of the figure show the bin limits in x for both Q^2 ranges. These points are placed in the middle of the bin. The curves indicate the GRV-HO (dotted), GRV-LO (solid), and SaS-1D (dashed) predictions for F_2^γ at the corresponding Q^2. The open symbols show results from other experiments at similar Q^2, with the total errors indicated only. These points are placed at the centre of the bins on a linear x scale.